IOPscience iopscience.iop.org

Home Search Collections Journals About Contact us My IOPscience

Toughened and machinable glass matrix composites reinforced with graphene and graphene-oxide nano platelets

This content has been downloaded from IOPscience. Please scroll down to see the full text.

2013 Sci. Technol. Adv. Mater. 14 055007

(http://iopscience.iop.org/1468-6996/14/5/055007)

View the table of contents for this issue, or go to the journal homepage for more

Download details:

IP Address: 129.120.87.225
This content was downloaded on 07/02/2017 at 17:17

Please note that terms and conditions apply.

You may also be interested in:

Toughness enhancement in graphene nanoplatelet/SiC reinforced Al2O3 ceramic hybrid nanocomposites
Iftikhar Ahmad, Mohammad Islam, Tayyab Subhani et al.

Carbon nanotube/silica composites obtained by sol–gel and high-pressure techniques
Mônica J de Andrade, Márcio D Lima, Carlos P Bergmann et al.

Incorporation of liquid-like multiwalled carbon nanotubes into an epoxy matrix by solvent-free processing
Ying-Kui Yang, Lin-Juan Yu, Ren-Gui Peng et al.

Nanomechanical characterization of single-walled carbon nanotube reinforced epoxycomposites
Xiaodong Li, Hongsheng Gao, Wally A Scrivens et al.

Dimethylformamide: an effective dispersant for making ceramic–carbon nanotubecomposites
Fawad Inam, Haixue Yan, Michael J Reece et al.

Recent advances in understanding the reinforcing ability and mechanism of carbon nanotubes in ceramic matrix composites
Mehdi Estili and Yoshio Sakka

The piezoresistive effect in graphene-based polymeric composites
A Tamburrano, F Sarasini, G De Bellis et al.

Unprecedented simultaneous enhancement in strain tolerance, toughness and strength of Al2O3 ceramic by multiwall-type failure of a high loading of carbon nanotubes
Mehdi Estili, Yoshio Sakka and Akira Kawasaki

OPEN ACCESS
IOP PUBLISHING
SCIENCE AND TECHNOLOGY OF ADVANCED MATERIALS
Sci. Technol. Adv. Mater. **14** (2013) 055007 (10pp)
doi:10.1088/1468-6996/14/5/055007

Toughened and machinable glass matrix composites reinforced with graphene and graphene-oxide nano platelets

Harshit Porwal[1,2], Peter Tatarko[3,6], Salvatore Grasso[1,2], Chunfeng Hu[4], Aldo R Boccaccini[5], Ivo Dlouhý[3] and Mike J Reece[1,2]

[1] School of Engineering and Material Science, Queen Mary University of London, London E1 4NS, UK
[2] Nanoforce Technology Limited, London, E1 4NS, UK
[3] Institute of Physics of Materials, ASCR, CEITEC IPM, Zizkova 22, 616 62 Brno, Czech Republic
[4] Ningbo Institute of Materials Technology and Engineering (NIMTE), Chinese Academy of Sciences (CAS), Ningbo 315201, People's Republic of China
[5] Department of Materials Science and Engineering, University of Erlangen-Nuremberg, Cauerstraße 6, D-91058 Erlangen, Germany

E-mail: m.j.reece@qmul.ac.uk

Received 8 July 2013
Accepted for publication 26 September 2013
Published 18 October 2013
Online at stacks.iop.org/STAM/14/055007

Abstract
The processing conditions for preparing well dispersed silica–graphene nanoplatelets and silica–graphene oxide nanoplatelets (GONP) composites were optimized using powder and colloidal processing routes. Fully dense silica–GONP composites with up to 2.5 vol% loading were consolidated using spark plasma sintering. The GONP aligned perpendicularly to the applied pressure during sintering. The fracture toughness of the composites increased linearly with increasing concentration of GONP and reached a value of ∼0.9 MPa $m^{1/2}$ for 2.5 vol% loading. Various toughening mechanisms including GONP necking, GONP pull-out, crack bridging, crack deflection and crack branching were observed. GONP decreased the hardness and brittleness index (BI) of the composites by ∼30 and ∼50% respectively. The decrease in BI makes silica–GONP composites machinable compared to pure silica. When compared to silica–Carbon nanotube composites, silica–GONP composites show better process-ability and enhanced mechanical properties.

Keywords: silica, graphene/graphene-oxide nanoplatelets, nanocomposites, mechanical properties, sintering

1. Introduction

Graphene is being considered as a reinforcing agent for various composite systems due to its mechanical, electrical and thermal properties [1–3]. Graphene itself has found applications in various fields including lithium ion batteries, bio-sensors, transparent conductors and super capacitors [4–7]. There is a considerable amount of work reported in the literature on polymer-graphene composites [8–14], but the use of graphene for preparing reinforced metal, ceramic and glass [15–18] matrices composites is relatively new.

The majority of the work on ceramic composites in the last decade has been focused on carbon nanotube (CNT) reinforced inorganic (glass and ceramic) matrix composites [19–25] because of their attractive combination of mechanical and multifunctional properties [26–28].

[6] Current affiliation: Institute of Materials Research, Slovak Academy of Sciences, Watsonova 47, 04001 Kosice, Slovak Republic.

Content from this work may be used under the terms of the Creative Commons Attribution-NonCommercial-ShareAlike 3.0 licence. Any further distribution of this work must maintain attribution to the author(s) and the title of the work, journal citation and DOI.

 © 2013 National Institute for Materials Science Printed in the UK

However, graphene apart from having similar properties to CNTs also has additional advantages such as: high specific surface area [29]; and less tendency to tangle, which makes it easier to disperse in a matrix (whereas CNTs usually require surface modification [20]). Graphene is also relatively easy to produce, inexpensive and potentially less toxic compared to CNTs [30]. Recently Tapaszto *et al* [31]. compared the mechanical properties of silicon nitride–CNTs and silicon nitride-graphene composites with 3 wt% loading. According to their results, graphene was easy to process and disperse compared to CNTs, it also produced better mechanical properties. Similarly Walker *et al* [32] reported an improvement of ∼235% in fracture toughness of silicon nitride–graphene (1.5 vol%) composites, while Fan *et al* [33] reported an electrical conductivity of 1000 S m^{-1} with the addition of only 2.35 vol% graphene to an alumina matrix. In view of these encouraging results, the use of graphene to produce reinforced inorganic matrix composites has great unexplored potential.

In the present study, graphene nanoplatelets (GNP) and graphene oxide nanoplatelets (GONP) reinforced silica composites were prepared. Firstly, dispersion of GNP and GONP in the silica matrix were optimized with reproducible results using different processing routes, namely powder and colloidal processing. Secondly, composites with different volume fraction of GONP were prepared and their mechanical properties characterized. Spark plasma sintering (SPS) was used to rapidly consolidate the composites, thus minimizing any structural damage to GNP and GONP during high temperature sintering [34]. The results and discussion make reference to the corresponding results reported in the literature for silica–CNTs composites [35]. Finally, the machinability of silica–GONP nanocomposites was investigated and compared with that of pure silica.

2. Experimental section

2.1. Synthesis of GNP

GNP was synthesized using a liquid phase exfoliation method. Graphite (Sigma Aldrich) was mixed with solvent *n*-methyl pyrrolidone (NMP) and sonicated (CV33 flat probe sonic tip, 50 W, 25 kHz) for 20 h in an ice bath. After synthesis the prepared GNP suspension was filtered using a vacuum filtration unit and re-dispersed in solvent dimethyl formamide (DMF) and sonicated for 20 min. After sonication, the suspension was centrifuged at 500 rpm for 45 min (Centurion Scientific) in order to remove the un-exfoliated graphite. The top 80% of the supernatant was separated by pipet after centrifugation [36]. It should be noted that NMP was used as a solvent for the exfoliation process because of its higher boiling point ∼200 °C, whereas DMF was used for processing of the powders because of its lower boiling point ∼80 °C thus enabling easy drying [37]. Also, commercially available GONP powder (Nano-Innova) was used to produce composites.

The prepared GNP was characterized using Transmission Electron Microscope (TEM) (JEOL JSM-2010, 200 kV), Raman (Renishaw inVia Raman microscope, laser power 12.5 mW, 514 nm argon laser) and UV–visible spectroscopy (Perkin Elmer-Lambda 950) as described elsewhere [36, 38, 39].

2.2. Composites powder preparation

In order to prepare homogeneous and well dispersed powder mixtures, two different processing routes were attempted: powder and colloidal processing. We tried fabricating composites using both GNP and GONP because they are expected to behave differently in the silica matrix. GONP is expected to show good dispersion and better interfacial bonding in the silica matrix compared to GNP.

2.2.1. Powder processing. To prepare well dispersed silica–GNP composite powders, the already prepared GNP suspension was diluted with DMF to a concentration of 1 mg ml^{-1} and sonicated using a sonication bath for 2 h. After sonication, commercially available silica powder (Sigma Aldrich, 20 nm) was added to the prepared suspension, and the slurry was ball milled at 350 rpm using a QM planetary ball mill (Nanjing University Instrument Plant) for 4 h with a powder-to-ball weight ratio of 1:20. After milling, the prepared slurry was dried on a hot plate at 80 °C for 12 h. The dried mixture was grounded and sieved using 250 mesh followed by drying in vacuum oven at 80 °C for another 2 days.

2.2.2. Colloidal processing. In order to prepare silica–GNP and silica–GONP composite powders using colloidal processing route, suspensions of GNP, GONP and silica were prepared separately. First, GNP/DMF [37] and GONP/ethanol suspensions were sonicated for 4 h in order to obtain good dispersion and exfoliation of GNP and GONP powders in the solvents. The concentrations of the suspensions were 1 mg ml^{-1}.

Similarly silica/DMF and silica/ethanol suspensions with concentrations 30 mg ml^{-1} were prepared by sonication for 2 h. Already prepared GNP and GONP suspensions were added drop wise to the silica suspensions with magnetic stirring (200 rpm). After 2 h of magnetic stirring suspensions were dried on a hot plate at 80 °C for 12 h. Similar to the powder processing method, the dried mixtures were ground and sieved using 250 mesh followed by drying in vacuum oven at 80 °C for another 2 days.

It should be noted that ethanol was used as a solvent for preparing GONP suspensions because in our initial experiments for preparing stable dispersions of GO using different solvents (DI water, ethanol) ethanol gave the best result. Zeta potential (Malvern Instrument-Nano ZS) measurements in the case of GONP and silica in ethanol gave the values of −5.36 and −5.61 mV respectively. Similar charge on the surface of both GONP and silica avoided the agglomeration of the particles during processing and helped in the good dispersion of GONP in the silica matrix. Similarly DMF was used as the processing solvent because of the good solubility of GNP in DMF.

2.3. Silica-GNP/GONP composites sintering and characterization

Silica–GNP and silica–GONP composites were densified using an SPS furnace (HPD 25/1, FCT systems, Germany, Furnace) at 1200 °C (heating, cooling rate 100 and 50 °C min^{-1} respectively) with simultaneous application of 50 MPa pressure for a dwell time of 7 min. The pressure was raised during heating (1100–1200 °C) from 12 to 50 MPa, and then linearly decreased in 6 min at 1200 °C. The samples were ground and polished using SiC papers down to 4000 grit and diamond suspensions. The bulk densities of the prepared composites were measured using Archimedes' method. The theoretical densities were estimated using the rule of mixtures and taking the densities of silica to be 2.2 g cm^{-3} and GNP, GONP to be 2.1 g cm^{-3} [14]. The dense composites were characterized using scanning electron microscope (SEM) (JEOL JSM-6300), x-ray diffraction (XRD) (Siemens Diffraktometer-D5000) and Raman spectroscopy.

The machinability of dense silica and silica–GONP composites was evaluated by drilling the polished samples using a high speed rotating WC-Co driller. The rotation speed of the drill was 560 rpm and the contact load was controlled by hand in order to inhibit the bending of drill. The drilled surfaces of the samples were examined by SEM.

2.4. Mechanical testing

2.4.1. Chevron notch fracture toughness measurements. The Chevron notch technique was used to determine the fracture toughness of the nanocomposites with the crack direction perpendicular to the oriented GONP. Chevron notches with the top angle of 90° were introduced into each bar (rectangular cross-section of 2 mm ×3 mm) as recommended for fracture toughness testing according to ASTM standard ASTM C142 (*standard Test Method for Determination of Fracture Toughness of Advanced Ceramics at Ambient Temperature, 2002*) using an ultra-thin diamond blade on a precision saw, Isomet 5000 (Buehler, USA). The reliability of this approach is described elsewhere [40]. A universal testing machine, Instron 8862 (USA), equipped with a three point bend test fixtures with a span of 16 mm, was used to apply the loading. A cross-head speed of 5 μm min^{-1} was used in all tests to achieve slow crack propagation during loading. An inductive extensometer was used to measure deflection, and force–deflection curves were recorded. The fracture toughness values were calculated by using the maximum force evaluated from the force–deflection curve and the specimen dimension using the following equation [35, 41].

$$K_{IC} = F_{max}/BW^{1/2}Y^*_{min}, \quad (1)$$

where Y^*_{min} is the minimum of geometrical compliance function, and B and W are the width and height of specimens, respectively. At least three beams were tested for each composite sample.

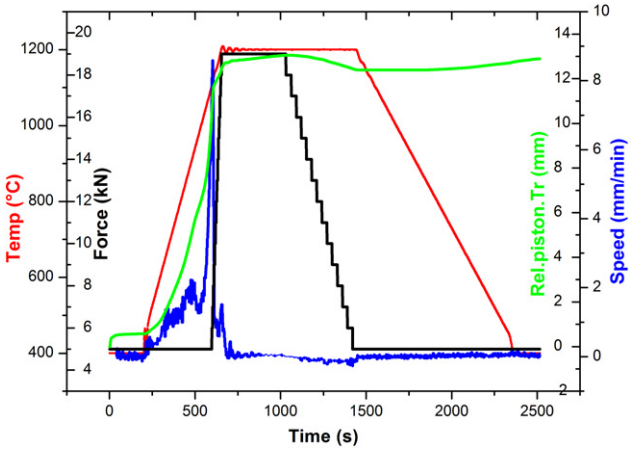

Figure 1. Sintering profile of silica during SPS processing (1200 °C per 50 MPa per 7 min). The relative piston travel and its speed refer to the upper ram movement as recoded by SPS machine.

2.4.2. Hardness and elastic modulus. The hardness values were measured on the polished cross-sections of bars using an instrumented indentation method with Vickers indenter. A standard loading/unloading test mode was used with a maximum load of 9.8 N (Zwick/Roell ZHU/Z2.5, Germany). The Martens hardness (HM) was calculated automatically by dividing the maximum test force P by the surface area of the indenter penetrating beyond the original surface of the test piece. It should be noted that because the properties of silica-GNP and silica-GONP composites were anisotropic due to alignment of GNP and GONP, all of the composites were tested on a surface with a normal parallel to the pressing direction of SPS.

The elastic modulus has been determined on the polished test bars $2 \times 3 \times 20$ mm^3 by the resonance method using GrindoSonic Mk5i (JW Lemmens N.V., Belgium) and at least ten readings were taken for each sample. Brittleness index (BI) was measured using equation

$$BI = HM/K_{IC}. \quad (2)$$

3. Results and discussion

Figure 1 shows relative piston travel, shrinkage rate, pressure and temperature profile recorded by the SPS furnace during sintering of pure silica. Silica–GNP and silica–GONP composites were prepared at 1200 °C [35]. The use of a short dwell time of 7 min avoided any structural damage of the GNP and GONP as determined by Raman spectroscopy. By analysing the sintering curves (not shown), no obvious change in the sintering behaviour was observed for silica–GNP and silica–GONP nanocomposites (0.5–2.5 vol%) in comparison to pure silica. As shown in figure 1, the powder started to densify at 500 °C and a sudden increase of the shrinkage was observed at 1100 °C due to the increased application of pressure.

Table 1 lists bulk and relative densities of the composites with 2.5 volume fraction of GNP and GONP. Density measurements confirmed that the composites were nearly fully dense. As seen in figure 2(a), the XRD patterns

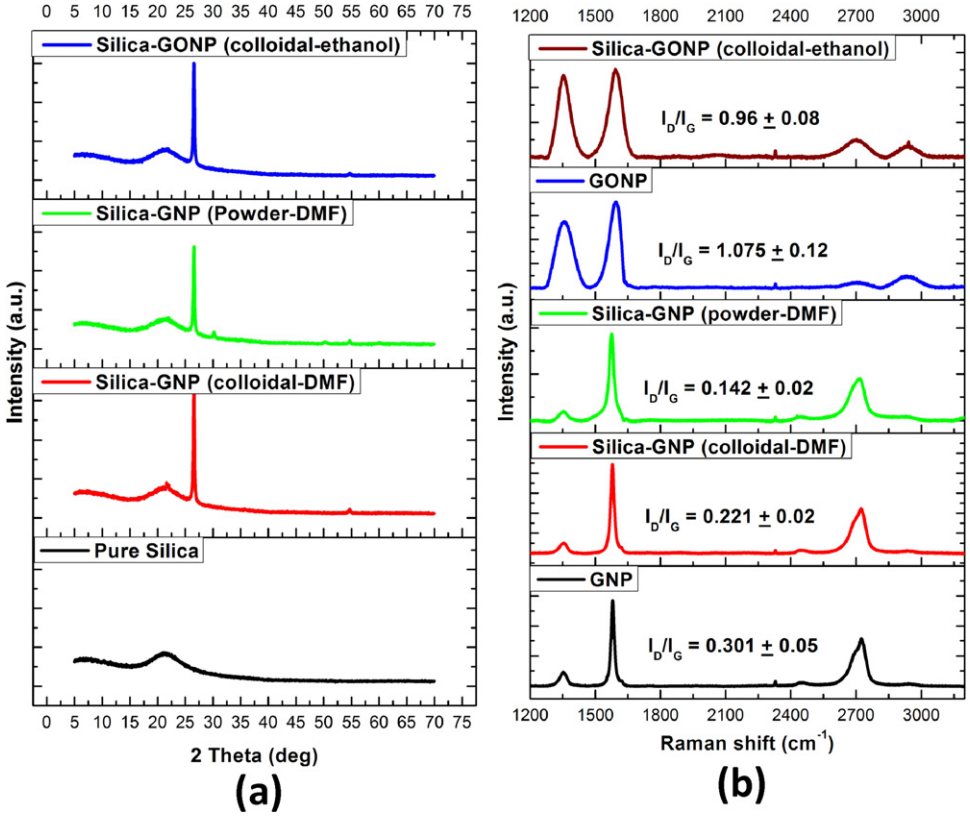

Figure 2. (a) XRD patterns and; (b) Raman spectra of GNP, GONP, silica–GNP and silica–GONP (2.5 vol%) nanocomposites prepared with different processing methods.

Table 1. Bulk and relative theoretical densities of prepared silica GNP/GONP (2.5 vol%) composites along with processing methods, solvents and sintering conditions. All the samples were sintered at 1200 °C under 50 MPa for 7 min. The quality of the GNP dispersion is also qualitatively described.

Sample	Bulk density ($g\,cm^3$)	% Relative density	Dispersion
SiO_2	2.18	99.2	–
SiO_2 + GNP (powder-DMF)	2.18	99.2	Fair
SiO_2 + GNP (colloidal-DMF)	2.12	96.3	Poor
SiO_2 + GONP (colloidal-ethanol)	2.19	99.4	Good

show completely amorphous phase for pure silica, and a crystalline carbon peak is observed at 26.3° for the silica–GNP and silica–GONP composites [42]. Also there is no detectable second phase or silica crystallization confirming that there was no reaction between silica and GNP/GONP during sintering. Raman spectroscopy was used to verify the structural integrity of both the GNP and GONP in the silica matrix after processing and sintering. The typical three peaks at $\sim$1350 cm^{-1} (D band), $\sim$1585 cm^{-1} (G band) and $\sim$2700 cm^{-1} (2D band) are observed for GNP and GONP [43] in figure 2(b). Raman spectra of pure GNP and GONP are compared to the silica–GNP and silica–GONP nanocomposites, and there is no detectable change in the position and intensity of D and G peaks, thus confirming that GNP and GONP were not damaged during sintering. Also the I_D/I_G ratio was slightly higher for GNP (0.3) than silica–GNP composites (0.22 and 0.14) respectively, suggesting that partial agglomeration of GNP during processing reduced the D peak intensity due to edge defects. Also I_D/I_G ratio of GONP (1.075) is higher compared to GNP (0.3) due to a reduction in size of sp^2 domains and an increase in sp^1 domains because of oxidation [44]. High temperature (1200 °C) processing in vacuum did not reduce the GONP to GNP, in fact there was no significant change in the I_D/I_G ratio for the starting GONP (1.075) compared with spark plasma sintered silica–GONP composites (0.98). Interestingly, silica–GONP composite were Raman inactive (figure not shown) when observed in the direction perpendicular to the SPS pressing. Thus, confirming the preferential alignment of GONP in the silica matrix.

In order to evaluate the quality of dispersion, the fracture surfaces of composites were investigated in SEM. Figure 3(a) shows GNP dispersed in the silica matrix using the powder processing method and DMF as solvent. It shows fair dispersion but, there was overlapping of GNP in the composite, which appeared thicker compared to the starting GNP [39]. The overlapping could have occurred during drying of the samples, and has been reported in literature by other researchers [33, 45]. Although good dispersion was observed in the case of powder processing, the absence of surface functional groups on GNP prevented any interaction between GNP and silica matrix during the powder processing resulting in overlapping of the flakes. Figure 3(b) shows

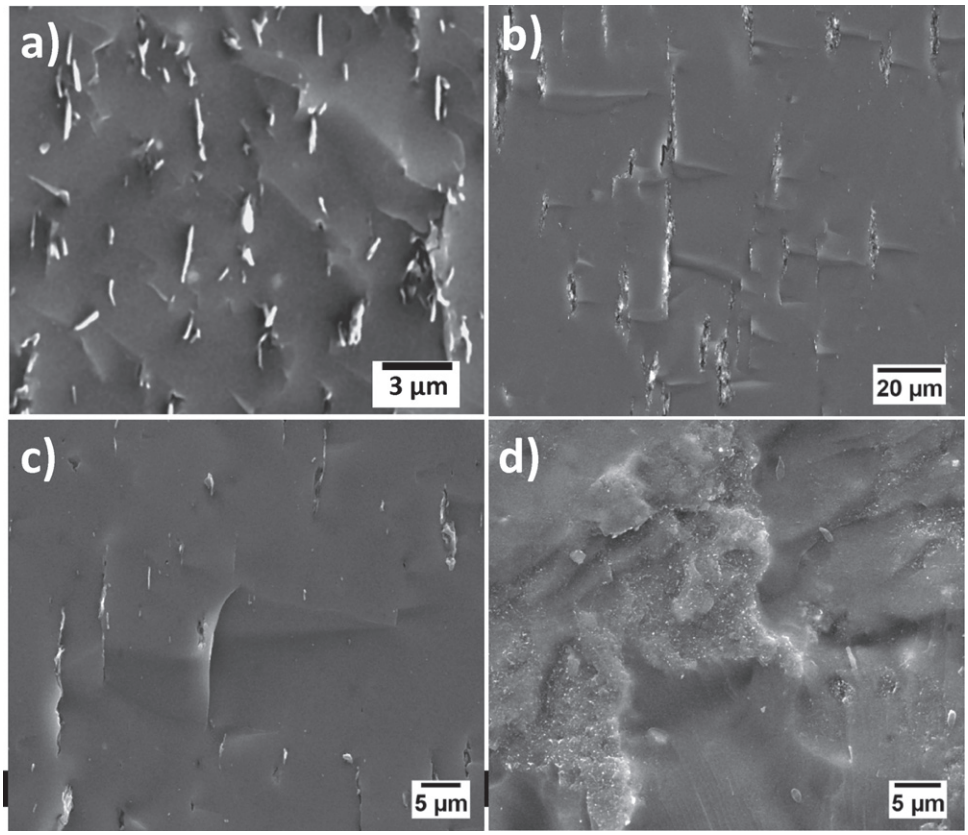

Figure 3. SEM images showing fractured surfaces of silica–GNP/GONP nanocomposites (2.5 vol%): (a) powder processing using GNP in DMF; (b) colloidal processing using GNP in DMF; (c) colloidal processing using GONP in ethanol and; (d) silica–CNT (2.5 vol%) composites prepared using powder processing and DMF as solvent. Pressure was applied in a direction perpendicular to the GNP/GONP orientation.

dispersion of GNP in silica matrix as prepared using the colloidal processing route and DMF as the solvent. The GNP is heavily agglomerated but these agglomerates are uniformly distributed throughout the silica matrix. It should be noted that no interaction between GNP and silica, and slow mixing (magnetic stirring) promoted agglomeration in the case of composites prepared using DMF and colloidal processing, while shear mixing during ball milling promoted good dispersion of GNP in the silica matrix, using DMF and powder processing route. In agreement with the density measurements in table 1, residual porosity was evident in the colloidally processed GNP composites, which was promoted by the GNP agglomerates and the associated interfacial cracking. Figure 3(c) shows dispersion of GONP in the silica matrix using the colloidal processing route and ethanol as the solvent. The best results were obtained with this method because the oxide layer in GONP tends to form good cohesive bonds with oxide matrices such as silica, thus avoiding undesired GONP overlapping. Interestingly, alignment of GNP and GONP was observed in the silica matrix in a direction perpendicular to the applied force. Alignment of the GNP and GONP can be attributed to their high specific surface area and two-dimensional (2D) geometry. The preferential alignment of GNP and GONP will result in anisotropic properties of the prepared composites [46]. In order to assess the ease of processability of GNP compared to CNTs, silica–GNP and silica–CNTs composites were prepared using

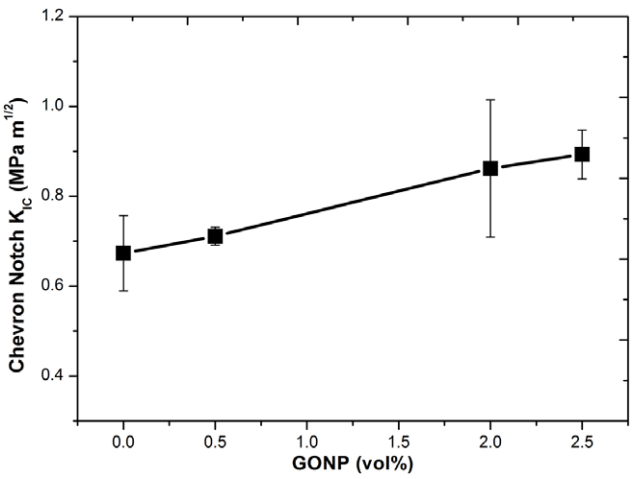

Figure 4. Fracture toughness of the silica–GONP nanocomposites measured with chevron notch fracture toughness method.

the powder processing route and DMF as the solvent (see experimental section). The results show that under similar processing conditions CNTs were heavily agglomerated and poorly dispersed (figure 3(d)), while on the contrary GNP exhibited good dispersion and alignment (figure 3(a)) in the silica matrix.

Silica–GONP composites prepared by colloidal processing showed the best dispersion results compared

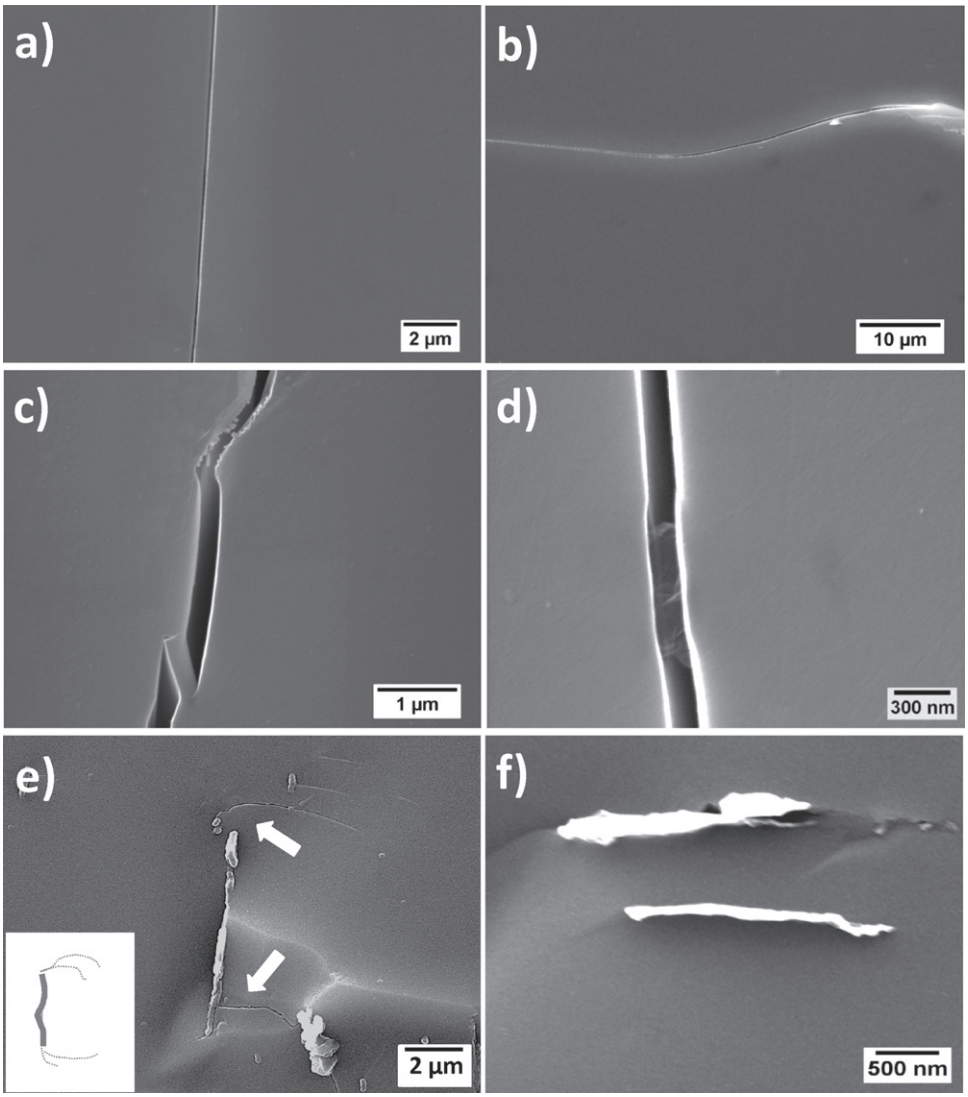

Figure 5. SEM fractured surface images of silica–GONP nanocomposites: (a) image showing straight crack path for pure silica; (b) low magnification image showing wavy crack path for silica-GONP nanocomposites; (c) crack deflection and GONP necking toughening mechanisms; (d) high magnification image showing GONP crack brigding; (e) chevron notch fractured surface image showing crack branching; and (f) GONP pull out from silica matrix.

to all of the composites. For this reason, nanocomposites with increasing content of GONP of 0.5, 2 and 2.5 vol% were prepared. The effect of GONP content on the fracture toughness of silica was investigated. A fracture toughness of 0.67 MPa m$^{1/2}$ was measured for pure silica sample. The fracture toughness of the composites increased linearly with increasing content of GONP (figure 4) and reached a value of 0.89 MPa m$^{1/2}$ for 2.5 vol% loading, corresponding to an increase of ∼35% compared to pure silica.

In order to understand the toughening mechanism of GONP compared to CNTs, the fracture toughness values of as prepared silica–GONP composites are compared to silica–CNTs composites from the literature, which were sintered, processed and characterized using similar conditions [35]. Silica–GONP composites had a toughness value of 0.89 MPa m$^{1/2}$ for 2.5 vol% loading while silica–CNTs composites had a similar value of 0.92 MPa m$^{1/2}$ for 7.5 wt% (9.67 vol%) loading, although the measured fracture toughness of pure silica was ∼0.6 MPa m$^{1/2}$ [35] compared to 0.67 MPa m$^{1/2}$ in the present work. Thus, in order to achieve a fracture toughness of about 0.9 MPa m$^{1/2}$, the necessary GONP loading was three times lower compared to CNTs. This suggests that GONP may be more effective than CNTs in improving fracture toughness. The easier processability and the improved mechanical properties of GONP composites can be attributed to high specific surface area; 2D geometry and better interfacial bonding of GONP compared to CNTs, which have a tendency to tangle and agglomerate.

4. Toughening mechanism

To investigate the toughening mechanisms of GONP in silica, fracture patterns generated from Vickers indentation were analysed. It was not possible to calculate fracture toughness and hardness values using the micro indentation (⩾ 5 kg)

Table 2. Physical and mechanical properties of silica–GONP nanocomposites.

Sample	Chevron notch K_{IC} (MPa m$^{1/2}$)	Martens hardness HM (GPa)	E-modulus (GPa)	Brittleness index (μm$^{-1/2}$)
SiO_2	0.67 ± 0.08	3.51 ± 0.14	71.3 ± 0.5	5.24
SiO_2 + GONP (0.5 vol%)	0.71 ± 0.02	3.07 ± 0.06	49.1 ± 0.9	4.32
SiO_2 + GONP (2 vol%)	0.86 ± 0.15	3.04 ± 0.08	48.6 ± 1.2	3.53
SiO_2 + GONP (2.5 vol%)	0.89 ± 0.05	2.55 ± 0.05	40.18 ± 1.4	2.86

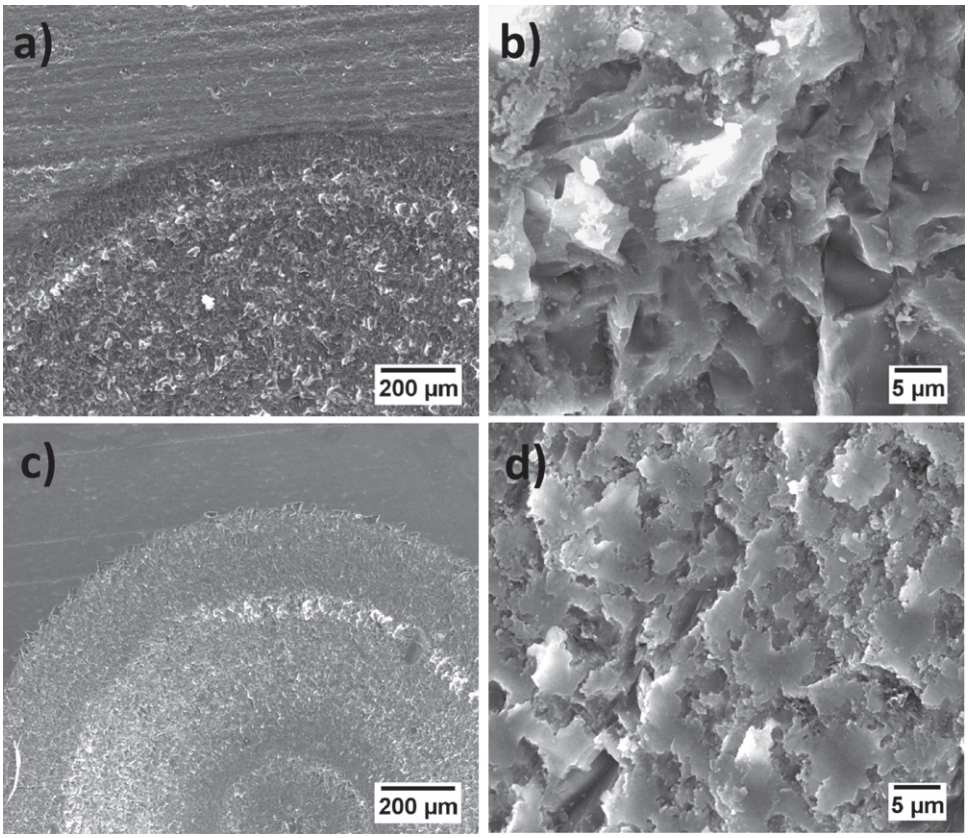

Figure 6. SEM images showing surfaces after drilling: (a) low, and (b) high magnification images for pure silica; and (c) low, and (d) high magnification images for silica-GONP (2.5 vol%) composite.

technique because indentation of glass did not generate a well-defined radial/median crack system, but instead chipped and produced ill-defined indentation impressions. By varying the loads (1, 2, 3 and 5 kg) radial cracks were observed. Figure 5 shows SEM images of Vickers indentation fracture surfaces for silica and silica-GONP nanocomposites. Figure 5(a) shows a typical straight crack path for pure silica. Figure 5(b) is the low magnification image showing the wavy crack path and figure 5(c) shows the deflected crack path in the case of silica–GONP (2.5 vol%) composites. GONP can be seen necking and joining the crack produced during indentation.

The differential thermal expansion between GONP and silica might have induced local stresses in the silica matrix enabling crack deflection. In fact, during cooling due to negative coefficient of thermal expansion of GONP [33, 47] it expands while silica contracts, generating high residual stresses [48]. These residual stresses might reduce the susceptibility of the glass to fracture. Figure 5(d) shows the anchoring of GONP in between the cracks showing GONP crack bridging toughening mechanism. Figure 5(e) shows fractured surface obtained by chevron notch showing crack branching toughening mechanism. When crack front interacts with GONP it deviates from its straight path. Crack is not able to propagate through the GONP so it is deflected. The crack deflection promotes energy dissipation through crack branching occurring along the edges of GONP. The inset of figure 5(e) depicts crack branching where GONP is sketched with grey colour and cracks shown with red colour. Crack branching toughening mechanism was observed in polycrystalline-graphene composites as reported in [49, 50]. It should be noted that crack deflection and crack branching were found to be the dominant toughening mechanisms. Figure 5(f) is the high magnification image showing GONP pull out from silica matrix. The nature of the interfacial bonding between GONP and silica plays an important role in toughening response. Due to the good interfacial bonding between the oxide layers of GONP and silica various toughening mechanism were observed for silica–GONP composites.

Table 2 summarizes the chevron notch fracture toughness, Martens hardness (HM), elastic modulus and BI values for silica–GONP nanocomposites. Analogous to CNTs, GONP reduces the elastic modulus and hardness of the glass composites with increasing concentration. The elastic modulus and hardness of the composite decreases by ∼45 and ∼30% respectively for 2.5 vol% silica GONP composite. In the case of CNTs, the reduction in hardness and Young's modulus with increasing concentration of CNTs was attributed to CNT agglomeration in borosilicate glass composites [23]. In the case of GONP silica glass composites, the reduction in both elastic modulus and hardness was even more marked because of the presence of relatively large and weakly bonded graphene planes.

BI can be used to quantitatively determine the machinability of glass ceramics [51]. The lower the BI, the higher the machinability of the glass-ceramics. Interestingly, the increase in fracture toughness and decrease in hardness remarkably decrease the BI of silica–GONP composites. As reported by Boccaccini, the BI of machinable glasses should be lower than $4.3\,\mu m^{-1/2}$ [51]. In the case of silica–GONP (2.5 vol%) composites the BI value decreased from 5.24 to $2.86\,\mu m^{-1/2}$, corresponding to a ∼50% decrease compared to pure silica. Figures 6 shows SEM micrographs of drilling indentations on the polished surface of pure silica and silica–GONP (2.5 vol%) composite. The silica-GONP composite exhibited good machinability. In comparison with pure silica, the drilled surface of composite was smoother and there was less debris. Under the shear stresses generated by drilling, the pure silica showed material removal mechanisms by fragmentation and fracture so that the drilled surfaces were coarse (figures 6(a) and (b)). During the drilling test, even under high loading of the drill, material removal was difficult. At longer drilling times, the drilling tip became red hot due to high friction. On the contrary, when drilling the GONP composites, it was found that the material removal was easier and the drilled surface was smoother and flat (figure 6(c) and (d)). As expected homogeneously distributed GONP flakes played an important role in dissipating the shear stresses and local heating in the silica matrix. Micro cracks were easy to emanate and propagate along the relatively weak GONP and silica matrix interface (figure 5). Also there was no significant local increase of temperature at the tip contact point (i.e. no red areas were observed). The addition of GONP produced a reduction in coefficient of friction [52–54] and an increase in thermal conductivity [46, 55] resulting in both reduced local heating and increased machinability.

5. Conclusions

To summarize, the processing conditions for preparing well dispersed silica–GNP and silica–GONP composites were optimized using different processing routes including powder and colloidal processing. Using the optimized conditions, well dispersed and fully dense (relative density >99%) silica–GONP composite powders were prepared using a colloidal processing route followed by SPS densification at 1200 °C with 50 MPa pressure. Alignment of GONP in the silica matrix was observed perpendicular to the pressing direction in SPS. There was an improvement of ∼35% in the fracture toughness of the composites with the addition of 2.5 vol% GONP as measured using the chevron notch fracture toughness method. Various toughening mechanism including GONP necking, GONP pull-out, crack bridging, crack deflection and crack branching were observed for silica–GONP composites. GONP induces local stresses in the silica matrix making cracks deviate from their normal straight path, increasing the fracture toughness of the composites. Hardness and BI of the composites decreases by ∼30 and ∼50% respectively compared to pure silica. The addition of GONP to silica matrix enhanced the machinability of silica-GONP composites. Silica–GONP composites show easy processability and better mechanical properties when compared to silica–CNTs composites. This can be attributed to the higher specific surface area and 2D geometry of GONP compared to CNTs, which have tendency to agglomerate. The present study suggests that GONP is an effective reinforcing agent to prepare tougher and machinable glass matrix composites.

Acknowledgments

The authors thank European Union's Seventh Framework Programme managed by REA-Research Executive Agency http://ec.europa.eu/research/rea (Marie Curie Action, GlaCERCo GA 264526) for their support and funding for this research. We are also grateful to Dr Mahesh Kumar Mani (Cardiff University, UK) for performing Raman measurements.

References

[1] Geim A K and Novoselov K S 2007 The rise of graphene *Nature Mater.* **6** 183–91
[2] Lee C, Wei X D, Kysar J W and Hone J 2008 Measurement of the elastic properties and intrinsic strength of monolayer graphene *Science* **321** 385–8
[3] Balandin A A 2011 Thermal properties of graphene and nanostructured carbon materials *Nature Mater* **10** 569–81
[4] Pumera M 2009 Electrochemistry of graphene: new horizons for sensing and energy storage *Chem. Rec.* **9** 211–23
[5] Mohanty N and Berry V 2008 Graphene-based single-bacterium resolution biodevice and DNA transistor: interfacing graphene derivatives with nanoscale and microscale biocomponents *Nano Lett.* **8** 4469–76
[6] Stoller M D, Park S J, Zhu Y W, An J H and Ruoff R S 2008 Graphene-based ultracapacitors *Nano lett.* **8** 3498–502
[7] Wu J B *et al* 2010 Organic light-emitting diodes on solution-processed graphene transparent electrodes *Acs Nano.* **4** 43–8
[8] Kuilla T, Bhadra S, Yao D H, Kim N H, Bose S and Lee J H 2010 Recent advances in graphene based polymer composites *Prog Polym. Sci.* **35** 1350–75
[9] Yasmin A, Luo J J and Daniel I M 2006 Processing of expanded graphite reinforced polymer nanocomposites *Compos. Sci. Technol.* **66** 1182–9
[10] Zheng W and Wong S C 2003 Electrical conductivity and dielectric properties of PMMA/expanded graphite composites *Compos Sci Technol.* **63** 225–35

[11] Kalaitzidou K, Fukushima H and Drzal L T 2007 Mechanical properties and morphological characterization of exfoliated graphite–polypropylene nanocomposites *Composites* A **38** 1675–82
[12] Stankovich S *et al* 2006 Graphene-based composite materials *Nature* **442** 282–6
[13] Liang J J *et al* Electromagnetic interference shielding of graphene/epoxy composites *Carbon* **47** 922–5
[14] Khan U, May P, Porwal H, Nawaz K and Coleman J N 2013 Improved adhesive strength and toughness of polyvinyl acetate glue on addition of small quantities of graphene *Acs Appl. Mater. Interface* **5** 1423–8
[15] Liu M C, Chen C L, Hu J, Wu X L and Wang X K 2011 Synthesis of magnetite/graphene oxide composite and application for cobalt(II) removal *J. Phys. Chem.* C **115** 25234–40
[16] Wang K, Wang Y F, Fan Z J, Yan J and Wei T 2011 Preparation of graphene nanosheet/alumina composites by spark plasma sintering *Mater Res Bull.* **46** 315–8
[17] Zhu J T, Wong H M, Yeung K W K and Tjong S C 2011 Spark plasma sintered hydroxyapatite/graphite nanosheet and hydroxyapatite/multiwalled carbon nanotube composites: mechanical and *in vitro* cellular properties *Adv. Eng. Mater.* **13** 336–41
[18] Porwal H, Grasso S and Reece M 2014 Review of graphene–ceramic matrix composites *Adv. Appl. Ceram.* at press (doi 10.1179/1743676113Y.0000000095)
[19] Hwang G L and Hwang K C 2001 Carbon nanotube reinforced ceramics *J. Mater. Chem.* **11** 1722–5
[20] Cho J, Boccaccini A R and Shaffer M S P 2009 Ceramic matrix composites containing carbon nanotubes *J. Mater. Sci.* **44** 1934–51
[21] Inam F, Yan H X, Jayaseelan D D, Peijs T and Reece M J 2010 Electrically conductive alumina–carbon nanocomposites prepared by Spark Plasma Sintering *J. Eur. Ceram. Soc.* **30** 153–7
[22] Boccaccini A R, Thomas B J C, Brusatin G and Colombo P 2007 Mechanical and electrical properties of hot-pressed borosilicate glass matrix composites containing multi-wall carbon nanotubes *J. Mater. Sci.* **42** 2030–6
[23] Thomas B J C, Shaffer M S P and Boccaccini A R 2009 Sol–gel route to carbon nanotube borosilicate glass composites *Composites* A **40** 837–45
[24] Milsom B, Viola G, Gao Z P, Inam F, Peijs T and Reece M J 2012 The effect of carbon nanotubes on the sintering behaviour of zirconia *J. Eur. Ceram. Soc.* **32** 4149–56
[25] Inam F, Yan H X, Peijs T and Reece M J 2010 The sintering and grain growth behaviour of ceramic–carbon nanotube nanocomposites *Compos. Sci. Technol.* **70** 947–52
[26] Treacy M M J, Ebbesen T W and Gibson J M 1996 Exceptionally high Young's modulus observed for individual carbon nanotubes *Nature* **381** 678–80
[27] Ruoff R S and Lorents D C 1995 Mechanical and thermal-properties of carbon nanotubes *Carbon* **33** 925–30
[28] Thess A *et al* 1996 Crystalline ropes of metallic carbon nanotubes *Science* **273** 483–7
[29] Fan Y C *et al* 2010 Preparation and electrical properties of graphene nanosheet/Al_2O_3 composites *Carbon* **48** 1743–9
[30] Lam C W, James J T, McCluskey R, Arepalli S and Hunter R L 2006 A review of carbon nanotube toxicity and assessment of potential occupational and environmental health risks *Crit. Rev. Toxicol.* **36** 189–217
[31] Tapaszto O, Tapaszto L, Marko M, Kern F, Gadow R and Balazsi C 2011 Dispersion patterns of graphene and carbon nanotubes in ceramic matrix composites *Chem. Phys. Lett.* **511** 340–3
[32] Walker L S, Marotto V R, Rafiee M A, Koratkar N and Corral E L 2011 Toughening in graphene ceramic composites *Acs Nano* **5** 3182–90
[33] Fan Y C, Jiang W and Kawasaki A 2012 Highly conductive few-layer graphene/Al_2O_3 nanocomposites with tunable charge carrier type *Adv. Funct. Mater.* **22** 3882–9
[34] Inam F, Yan H, Reece M J and Peijs T 2010 Structural and chemical stability of multiwall carbon nanotubes in sintered ceramic nanocomposite *Adv. Appl. Ceram.* **109** 240–5
[35] Cho J *et al* 2011 Carbon nanotubes: do they toughen brittle matrices? *J. Mater. Sci.* **46** 4770–9
[36] Khan U, O'Neill A, Porwal H, May P, Nawaz K and Coleman J N 2012 Size selection of dispersed, exfoliated graphene flakes by controlled centrifugation *Carbon* **50** 470–5
[37] Inam F, Yan H, Reece M J and Peijs T 2008 Dimethylformamide: an effective dispersant for making ceramic–carbon nanotube composites *Nanotechnology* **19** 195710
[38] Khan U, Porwal H, O'Neill A, Nawaz K, May P and Coleman J N 2011 Solvent-exfoliated graphene at extremely high concentration *Langmuir* **27** 9077–82
[39] Porwal H, Tatarko P, Grasso S, Khaliq J, Dlouhý I and Reece M 2013 Graphene reinforced alumina nano-composites *Carbon* **64** 359–69
[40] Boccaccini A R, Rawlings R D and Dlouhy I 2003 Reliability of the chevron-notch technique for fracture toughness determination in glass *Mater. Sci. Eng.* A **347** 102–8
[41] Dlouhy I, Holzmann M, Man J and Valka L 1994 The use of chevron-notched specimens for fracture-toughness determination of bearing steels *Kov. Mater.* **32** 3–13
[42] Wu Y P *et al* 2010 Efficient and large-scale synthesis of few-layered graphene using an arc-discharge method and conductivity studies of the resulting films *Nano Res.* **3** 661–9
[43] Ramirez C and Osendi M I 2013 Characterization of graphene nanoplatelets–Si_3N_4 composites by Raman spectroscopy *J. Eur. Ceram. Soc.* **33** 471–7
[44] Stankovich S *et al* 2007 Synthesis of graphene-based nanosheets via chemical reduction of exfoliated graphite oxide *Carbon* **45** 1558–65
[45] Liu J, Yan H and Jiang K 2013 Mechanical properties of graphene platelet-reinforced alumina ceramic composites *Ceram Int.* **39** 6215–21
[46] Miranzo P, Garcia E, Ramirez C, Gonzalez-Julian J, Belmonte M and Osendi M I 2012 Anisotropic thermal conductivity of silicon nitride ceramics containing carbon nanostructures *J. Eur. Ceram. Soc.* **32** 1847–54
[47] Mounet N and Marzari N 2005 First-principles determination of the structural, vibrational and thermodynamic properties of diamond, graphite, and derivatives *Phys. Rev. B* **71** 205214
[48] Yoon D, Son Y W and Cheong H 2011 Negative thermal expansion coefficient of graphene measured by Raman spectroscopy *Nano Lett.* **11** 3227–31
[49] Kvetkova L, Duszova A, Hvizdos P, Dusza J, Kun P and Balazsi C 2012 Fracture toughness and toughening mechanisms in graphene platelet reinforced Si_3N_4 composites *Scr. Mater.* **66** 793–6
[50] Dusza J *et al* 2012 Microstructure and fracture toughness of Si_3N_4 + graphene platelet composites *J. Eur. Ceram. Soc.* **32** 3389–97
[51] Boccaccini A R 1997 Machinability and brittleness of glass-ceramics *J. Mater. Process. Technol.* **65** 302–4

[52] Kim H J and Kim D E 2012 MD simulation of the frictional behavior of CNTs with respect to orientation *Tribol. Int.* **50** 51–6

[53] Liu Y H, Wang X K, Pan G S and Luo J B 2013 A comparative study between graphene oxide and diamond nanoparticles as water-based lubricating additives *Sci. China Technol Sci.* **56** 152–7

[54] Porwal H *et al* 2013 Tribological properties of silica–graphene nano platelet composites (in preparation)

[55] Yu Z T *et al* 2013 Increased thermal conductivity of liquid paraffin-based suspensions in the presence of carbon nano-additives of various sizes and shapes *Carbon* **53** 277–85